

A Comparative Study of Carbon Nanotubes and Graphene Nanoplatelets on Structure-Property Relationship of Aluminium Matrix Composites Synthesized by Spark Plasma Sintering



Mahmood Khan, Muhammad Shahzad, Muhammad Abdul Basit, Rafi Ud Din, Shahid Akhtar, Syed Wilayat Husain, and Ragnhild Elizabeth Aune

Abstract The fabrication of aluminium matrix composites with lightweight nanor-inforcements has proven to be very attractive due to their superior properties. In the present study, Carbon Nanotubes (CNTs) and Graphene Nanoplatelets (GNPs) have been incorporated into an aluminium matrix using the Spark Plasma Sintering (SPS) process. Composite samples with varying amounts of CNTs and GNPs (0.1–0.5 wt.%) were prepared and the effect on the mechanical properties was investigated. The microstructural evolution and the yield strength of each sample were evaluated and compared with neat reference samples. It was established that the CNT reinforced nanocomposites exhibited a relatively higher yield strength than the GNP reinforced. An improvement by 13% and 18%, respectively, for additions of 0.5 wt.% CNTs was found. Based on the experimental results, the presence of a 2D planer geometry is modelled and discussed in view of its ability to enable a more efficient network at low wt.% of the fillers.

Keywords Spark plasma sintering (SPS) · Carbon nanotubes (CNTs) · Graphene nanoplatelets (GNPs) · Aluminium matrix composite (AMCs) · Mechanical properties · Microstructure

M. Khan (✉) · R. E. Aune

Department of Materials Science and Engineering, Norwegian University of Science and Technology (NTNU), Trondheim, Norway
e-mail: mahmood.khan@ntnu.no

M. Shahzad · R. U. Din

Materials Division, Pakistan Institute of Nuclear Science and Technology, Nilore 45650, Pakistan

M. A. Basit · S. W. Husain

Department of Materials Science and Engineering, Institute of Space Technology, Islamabad 44000, Pakistan

S. Akhtar

Hydro Aluminium AS, Research and Technology Development, Karmøy, Norway

Introduction

The prospects of lightweight AMCs have wide potential in the aerospace and automotive industries due to their improved mechanical properties. In recent times, there has been a lot of focus on carbonaceous nanoreinforcements for improvements in the properties of aluminium and its alloys [1]. In these studies, CNTs and GNPs are the predominant choices of nanoreinforcements mainly due to availability, cost, and ease of processing. Aluminium matrix composites (AMCs) exhibit improvements and their properties could be tailored for a specific set of applications [2]. AMCs are getting popular in industries like to meet performance and economic benefits [3]. Carbonaceous nanoreinforcements, compared to ceramic counterparts such as boron carbide (B_4C), titanium carbide (TiC), silica (SiC), alumina (Al_2O_3), aluminium nitride (AlN), etc., pose difficulty in dispersion in the aluminium matrix [4].

The addition of CNTs in the aluminium matrix has been reported to increase matrix mechanical strength by appreciable fraction [5]. Similarly, GNPs have also been beneficial up to a certain extent in the aluminium matrix [6]. The choice of weight fraction introduced in the aluminium matrix greatly depends on the composite processing technique [7]. Various processing methods have been chosen and customized to overcome the wetting issue of carbonaceous nanoreinforcements in the aluminium matrix. Among these methods are powder metallurgy (PM) with pressure-less and pressure-assisted sintering, stir casting also termed as vortex casting, squeeze casting, pressure infiltration, friction stir processing [8]/welding [9], spark plasma sintering (SPS) [8–15], etc. The main factor in connection with the dispersion of CNTs and GNPs is the preliminary dispersion procedure added in the process before final compaction/consolidation.

Secondary processing techniques mainly affect the final density of the resulting composite [16]. Generally, solid-state processing via powder metallurgy is preferred due to better dispersion and lower processing temperatures compared to liquid processing [17, 18]. The variety of secondary processing techniques like forging, rolling, extrusion, and hot pressing are costly choice for the manufacturing of AMCs [19–22]. The application of a secondary processing step should address two issues, namely, optimization of density and microstructure of the final composite and prevent the formation of unnecessary phases/intermetallics [23, 24]. SPS has attracted the attention of researchers over the past few years for AMCs synthesis/production. The plasma associated with the flow of charge limits the time of sintering compared to the conventional PM sintering [25]. Simultaneous application of pressure assists compaction to ensure near-theoretical densities of SPS composites [26]. The confined generation of heat due to the flow of charge at the mating surfaces of the powders also results in the removal of the oxide layer [27]. These distinct features make SPS a more feasible and cost-effective choice for AMCs synthesis.

One of the aims of this study is to develop AMCs with CNTs and GNPs processed by optimized ball milling, cold compaction, and ultimately SPS. The nanoreinforced SPSed composites were characterized by optical, scanning electron spectroscopy, X-Ray diffraction (XRD), microhardness, and tensile tests.

Experimentation

Materials

Aluminium powder of spherical morphology and nominal particle size of $\sim 20 \mu\text{m}$ was used as a matrix [6]. The matrix powder particle size was measured by Mastersizer 3000, Malvern Instruments, UK. The composition of the aluminium matrix powders was confirmed by Inductively Coupled Plasma Mass Spectroscopy (ICPMS), as shown in Table 1. CNTs and GNPs were purchased from Hongwu International Group, China. The CNTs were multi-walled with an estimated length of $1 \mu\text{m}$ and diameter of 20–30 nm [8]. Average thickness and GNPs length estimated from scanning electron microscopy (SEM) are around 1–5 μm , and 5–10 nm, respectively [10]. All the raw materials characterization and morphological details are published elsewhere.

Composite Processing

CNTs and GNPs were acid-treated for functionalization prior to sonication with aluminium powder. Functionalization of 0.25 g of CNTs and 0.25 g GNPs was carried out separately by dispersing them in 80 ml of 16 M concentrated HNO_3 followed by sonication in the ultrasonic bath (Bransonic, Thomas Scientific, USA) for 2 h at 40°C . Later the mixture was diluted with distilled water and filtered through laminated PTFE filters (GVS, Zona Industriale, Italy). The filtered cake samples of CNTs and GNPs were washed with distilled water until the pH was raised to 7. The CNT and GNP mixtures were dried in an oven for 8 h [28]. The weighed quantities from these functionalized mixtures of CNTs and GNPs (as per their respective composite group in Table 1) were then dispersed in 70/30% water/ethanol solution [29]. The mixtures were again sonicated in the UP400S probe sonicator (Hielscher, GmbH) for 30 min at a frequency of 24 kHz. The corresponding weighed quantity of Al6061 matrix powder was added to the solution followed by sonication for 15 min [30].

RETSCH planetary ball mill PM-100 was used with zirconia cylindrical balls for milling. The ratio of the grinding media mass to the milling composite mass was 20:1. The details of ball milling parameters were chosen from [31]. All the ball-milled powders were initially precompacted at 150 MPa in a graphite die with the hydraulic press (Big Red™ 10, Torin® USA). The final consolidation along with sintering was achieved by sintering in SPS—825 (Dr. Sinter, Fuji Electronic Ltd. Japan). Table 1 shows the SPS parameters utilized to achieve near-theoretical densities. Five samples of reference and each composition as per Table 1 were prepared. Figure 1 shows schematics of the fabrication process of reference and composite samples incorporating SPS.

Table 1 Details of Al6061 showing: **a** nominal composition in wt.% as measured from ICPMS, **b** SPS parameters, and **c** description of SPS reference and composites

a) Nominal composition of Al6061 powder						
	Mg	Si	Cu	Cr	Fe	Zn
Al6061	1.04	0.55	0.26	0.07	0.04	0.003
b) SPS parameters						
Temperature	Pressure	Heating rate	Holding time	Vacuum		
450 °C	60 MPa	50 °C/min	10 min	10 Pa		
c) Composites description used in the manuscript						
Sr. no.	Sample	Description				
1	Al6061	Reference sample				
2	Al6061-0.1 CNTs	0.1 wt.% CNTs in Al6061 matrix				
3	Al6061-0.5 CNTs	0.5 wt.% CNTs in Al6061 matrix				
4	Al6061-0.1 GNPs	0.1 wt.% GNPs in Al6061 matrix				
5	Al6061-0.5 GNPs	0.5 wt.% GNPs in Al6061 matrix				

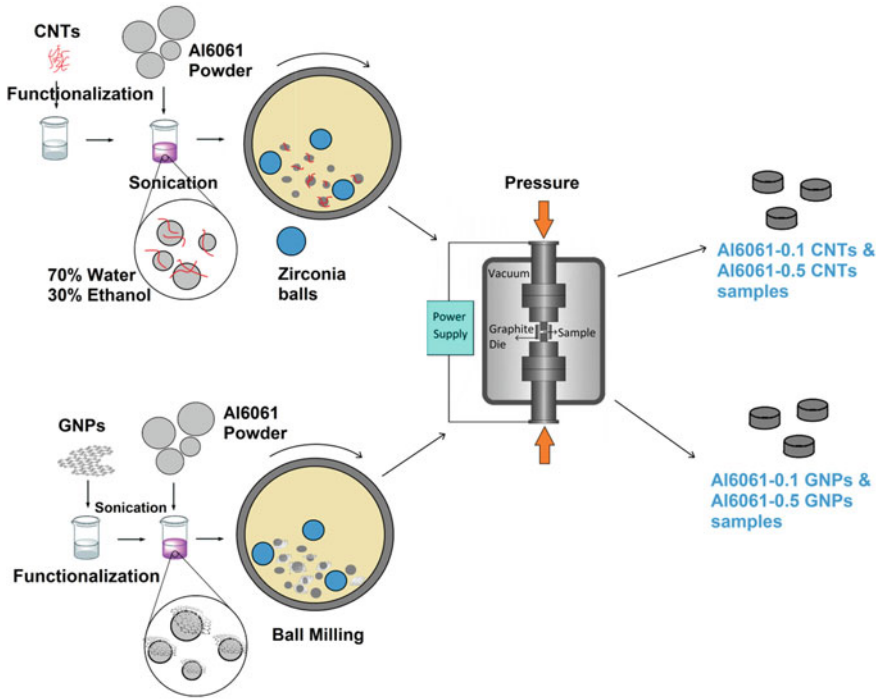


Fig. 1 Schematics of the process used for the synthesis of Al6061 composites with CNT and GNP reinforcements incorporating ball milling and SPS

Characterization

Metallographic samples preparation of all the samples after the SPS procedure was carried out by cutting them with silicon carbide cut-off wheel 10S15 on struers accutom-5. The samples were then mounted in epoxy for grinding and polishing operations. Grinding papers of grit sizes 500, 800, 1200, 2400, and 4000 were used on RotoPol-31 and RotoForce-4 (Struers, Denmark). Later Tegramin-30 with DiaPro Mol3, DiaPro Nap-B1, and OP-S were used for polishing. Zeiss AXIO Scope.A1 (ZEISS, Germany) polarizing microscope was used for optical microstructural analysis after etching. Keller’s reagent (150 ml H₂O, 5 ml HNO₃, 3 ml HCl, and 2 ml HF) was used as an etchant for the polished surfaces of reference and composite samples.

SEM analysis was performed on SUPRA 55VP (ZEISS, Germany) equipped with EDAX Octane Pro-A (AMETEK, Inc., USA) which was used for EDS of composite powders and polished samples (after SPS). For crystallographic examination and the possible existence of intermetallic phases, XRD was performed on DaVinci D8 Advance X-Ray Diffractometer (Bruker, USA). The reference and composite samples were scanned from 10 to 80° @ 0.2° resolution angle.

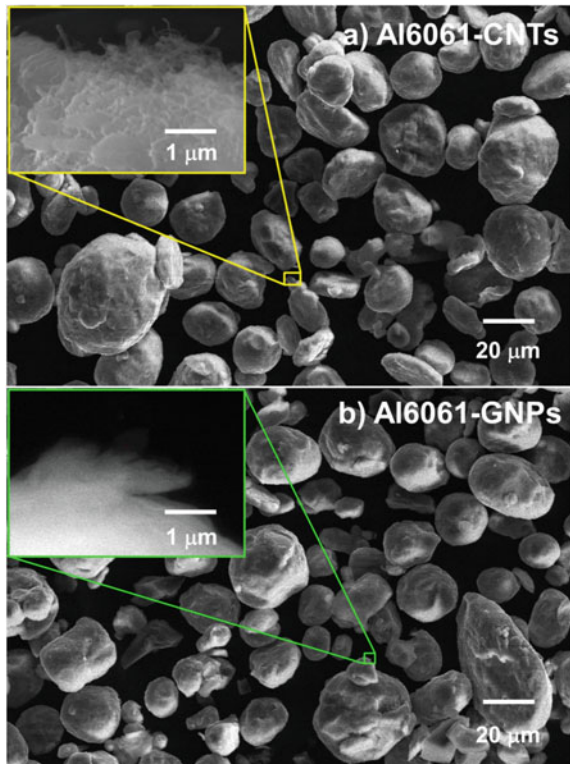
Hardness and compression tests were carried out to assess the mechanical properties of the reference and composite samples. For the hardness test, HMV-G 21DT (Shimadzu, Japan) was used at a test load of 490.3 mN (HV 0.05) and a dwell time of 6 s. The compression tests were performed on MTS 880 universal testing machine (10 tons), equipped with MTS Teststar to control unit. The specimen size was around $8 \times 5 \times 5$ mm in length \times width \times thickness, respectively. The strain rate of 1 mm/min was selected via the machine crosshead movement method.

Results and Discussion

Composite Powders

Figure 2 shows the SEM images of the CNT- and GNP-based composite powders after ball milling operation. The low fraction of both nanoreinforcements in the aluminium matrix makes them difficult to visualize. Other contributing factors in

Fig. 2 SEM images of the ball-milled composite powders containing: **a** 0.5 CNTs and **b** 0.5 GNP



making the nanoreinforcements visually impaired can be (1) entanglement and exfoliation of the CNTs and GNPs during functionalization, solution sonication, and ball milling; (2) uniform distribution in the Al6061 matrix powders; and (3) inherent transparent nature of carbonaceous nanoreinforcements. The degree of deformation can be witnessed by comparing it with the raw spherical morphology of the matrix powder. Wear and tear marks embed CNTs and GNPs in their respective compositional composites. Ball milling parameters were optimized to avoid mechanical alloying to avoid segregation of carbonaceous nanoreinforcements due to density basis. No major difference could be noticed between the CNT and GNP composites. However, Fig. 2 shows a higher degree of aluminium matrix particle wrapping compared to CNTs.

Composites Densities

The theoretical densities of all the samples were calculated by Eq. (1), commonly known as the rule of mixture [32]:

$$\rho_{RC} = \rho_N V_N + \rho_M V_M \quad (1)$$

where “ ρ ” is the density and “ V ” is the volume fractions (0.1–0.5%) and the subscripts “RC”, “N”, and “M” symbolize the reference/composite, CNTs/GNPs, and Al6061 matrix, respectively. The experimental densities were measured by the Archimedes method. Figure 3 shows the density values plotted with respective reinforcement contents in the Al6061 matrix. The addition of lower density reinforcements, i.e., CNTs and GNPs, in the Al6061 matrix results in a decrease of composite density. Therefore, a decreasing trend is evident from the plotted values of Table 2.

Fig. 3 Theoretical and experimental densities plotted with wt.% of CNT and GNP composites along with the reference

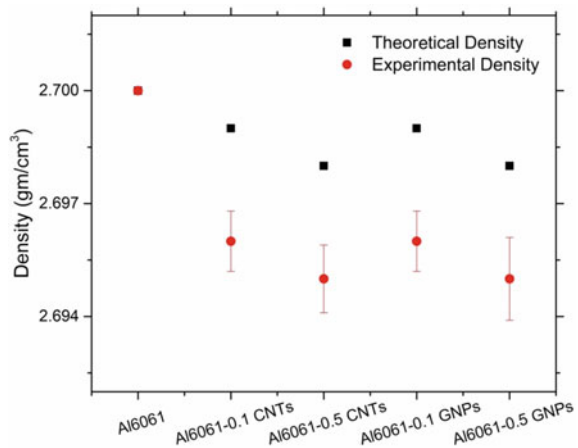


Table 2 Properties of SPS reference and CNT/GNP composites

Description	Theoretical density (gm/cm ³)	Experimental density (gm/cm ³)	Avg. grain diameter (µm)	ASTM(#)	Grain/mm(#)	Hardness		Compressive strength		Failure strain	
						Hv	Std. dev. (Hv)	MPA	Std. Dev. (MPa)	%	Std. Dev. (%)
Al6061	2.7	2.7 ± 0.0	12.45	9.37	80.3	45	±2	90	±6	-	-
Al6061-0.1CNTs	2.699	2.696 ± 0.001	11.92	9.49	83.8	49	±2.5	98	±6	35	±2.5
Al6061-0.5CNTs	2.698	2.695 ± 0.001	11.88	9.52	84.4	51	±3.5	107	±8	24	±3.5
Al6061-0.1GNPs	2.699	2.695 ± 0.001	11.80	9.53	84.9	48	±3	95	±8	25	±3
Al6061-0.5GNPs	2.698	2.693 ± 0.002	11.71	9.55	85.6	50	±4	100	±10	18	±4

CNTs and GNPs exhibited the same effect on theoretical densities of the composites due to their approximately same weight fraction addition in the aluminium matrix. However, it can be noticed that at 0.5 wt.% GNPs-based composite has a lower density than the counterpart CNTs composite of the same weighted fraction. The lower experimental densities after SPS compared to the theoretical densities are mainly attributed to the non-wetting carbonaceous reinforcements with the metallic matrix [33]. This non-wet interface is expected to retain pores especially at higher fraction addition of nanoreinforcements.

Optical Microscopy

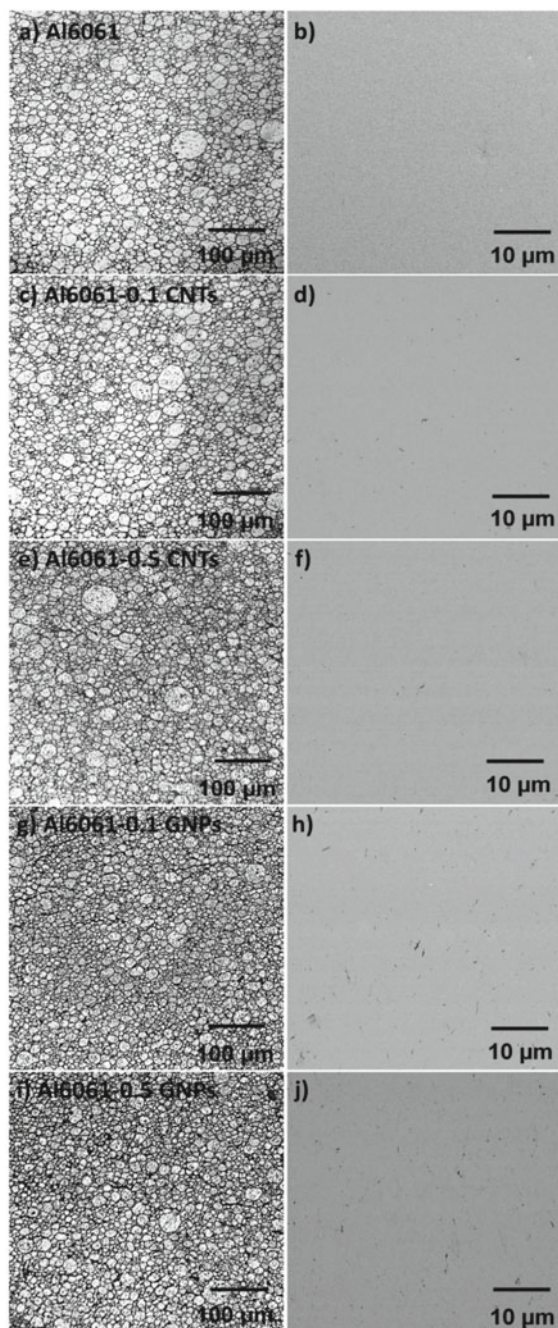
Figure 4 shows the optical and SEM micrographs of the Al6061 reference and SPS composites. Further details into microstructural analysis were carried out by measuring grain size in accordance with the Standard Test Methods for Determining Average Grain Size, Active Standard ASTM E112 (Developed by Subcommittee: E04.08ASTM), and Perfect Image™ (Clara Vision, France) software. The objective to carry out microstructure analysis was to (1) to investigate the densification of the processed samples, (2) effectiveness/extent of sintering, and (3) effect of nanoreinforcements on matrix and existence of any other phase developed/originated due to any possible matrix/reinforcement interaction.

No visual indications of any porosity were identified. Clear defect-free surfaces were observed as shown in Fig. 4. The microstructures show good densification of all the SPS reference (Fig. 4a and b) and composites samples (Fig. 4c–j). The composite samples with CNTs in 0.1 wt.% (Fig. 4c and d) and 0.5 wt.% (Fig. 4e and f) show randomly placed black dots in these OM images, which can be assumed to be the CNT clusters at the grain boundaries, as identified in Fig. 2a. The theoretical model is derived from the grains split illustration, showing the attachment of CNTs and GNPs on the Al6061 matrix. Carbonaceous nanoreinforcements are optically transparent and cannot be seen under optical microscopy on any polished and etched surface [1]. However, the agglomerated CNT/GNP lumps appear as dark spots or lines [3]. The intensity of these black dots increases in the GNP reinforced SPS composites, indicating a comparatively higher degree of pores. Figure 4g and 4h shows GNPs in 0.1 wt.% and Fig. 4i and j shows 0.5 wt.% GNP reinforced composites.

The presence of GNPs at the grain boundaries gives rise to micron-size pores, which is evident from the comparatively lower densities than CNT reinforced composites. From the grains size data as shown in Table 2, a decrease in the grain size is evident specifically due to the GNPs. The two-dimensional morphology of the GNPs compared to the unidirectional CNTs can lead to wrapping the matrix particles and finally resulting in a smaller grain size compared to the CNTs. The microstructure of the Al-GNP composites is greatly influenced by the GNP content in the matrix, sintering time, and temperature [34].

The presence of uniformly dispersed black spots in the OM images of the SPS composites indicates uniform dispersion of the nanoreinforcements which results in

Fig. 4 Optical and SEM micrographs of **a, b** reference, **c, d** Al6061-0.1 CNTs, **e, f** Al6061-0.5 CNTs, **g, h** Al6061-0.1 GNPs, **i, j** Al6061-0.5 GNPs



a decrease in the grain size [35]. The entrapment of CNTs and GNPs at the grain boundaries is mainly due to the deformation energy of the ball milling operation which consequently leads to mechanical alloying or cold welding of the matrix particles with each other and nanoreinforcements. Primarily, a two-colour contrast in the microstructures of the reference and composites shows no potential existence of any third coloured phase during the processing. XRD results are discussed in detail for the detection of any possible interphase or interfacial reactions at the reinforcement-matrix interface.

XRD

The XRD plots of the reference sample and all the CNT and GNP composites are shown in Fig. 5 (as per Table 1). Typical peaks of aluminium corresponding to face-centred cubic (FCC) crystals [36] can be seen at the respective 2θ plane positions. The intensity of the most closely packed (111) plane specific to FCC remains, as the maximum reflector of X-rays for the reference and the CNT/GNP composites. Other reflection peaks of XRD spectra of aluminium at their respective 2θ angles can be seen (2θ [200] = 45° , 2θ [220] = 65° , 2θ [331] = 78°) in Fig. 5. The low proportion of CNTs and GNPs yielded no peaks in any of the SPS composites. The XRD results in this work are in good agreement with the reported XRD measurements by W. M.

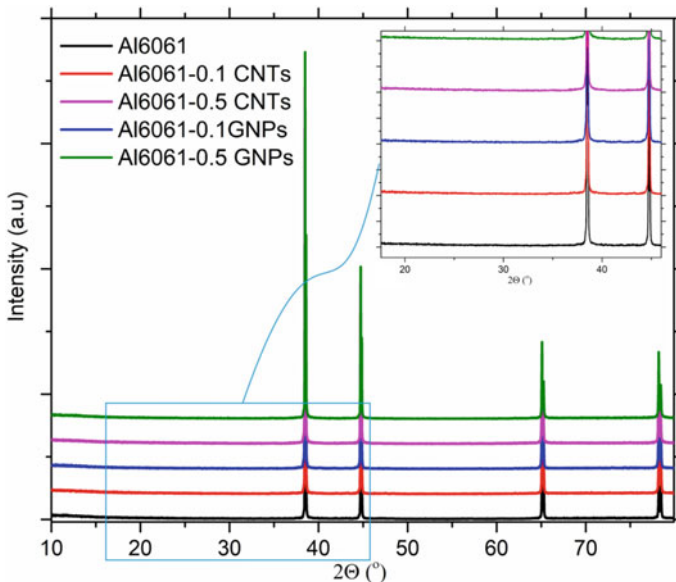


Fig. 5 XRD patterns of the SPS processed reference and all the composites in F and T6 conditions

Tian et al. [37]. The zoom-in section of the XRD plots shows no existence of any peak.

An earlier study by Bastros et al. [38] presented the detection limit of XRD for a lower fraction of secondary phases. Thus, the limitation of detection can be associated with the XRD diffractometer for not detecting CNTs and GNPs. The possible existence/formation of aluminium carbide (Al_4C_3) at $2\theta = 55^\circ$ can be ruled to be detected on this basis. Moreover, SPS is a unique processing method due to its plasma sintering with minimum time at higher temperatures compared to conventional sintering techniques. Yolshina et al. [39] reported the formation of Al_4C_3 at higher temperatures and pressure as achieved in hot pressing associated with longer sintering time.

Hardness

Table 2 shows the hardness values of the SPS processed, reference, and CNT and GNP composites. These values are plotted in Fig. 7 to represent the effect of carbonaceous nanoreinforcements on the bulk hardness of the composites. Six indents of Vickers indenter were made on each sample and error was noted as per Table 2. The baseline value was chosen of the reference sample which exhibited 45 ± 2 HV. Incorporation of 0.1 wt.% CNTs and GNPs in the Al6061 matrix added a 9% and 7% increase in the hardness of the composite, respectively (Fig. 7). An incremental increase in the hardness of the matrix due to the presence of CNTs and GNPs has also been reported earlier by Salama et al. [40] and Latief et al. [41], respectively.

Further addition of 0.5 wt.% CNTs and GNPs, respectively, increases 13 and 11% hardness of the Al6061 matrix. The contribution of CNTs in an increase of hardness is one of the main findings of this study. The comparative approach has allowed us to propose certain facts related to the contribution of carbonaceous nanoreinforcements in the strengthening of the aluminium matrix. A general increase in the hardness of the CNT/GNP composites can be explained with the help of thermal mismatch concepts of the reinforcements and matrix. The stresses are generated by the presence of a carbonaceous reinforcement in a metallic matrix. The nanoreinforcement stresses the matrix phase by adding dislocations and strain fields, as a second phase in the matrix [42], thereby generating a non-equilibrium state dispersed uniformly/evenly in the matrix.

Comparing the hardness of CNT reinforced composites with GNP reinforced composites, a noticeable decrease is evident which can be explained by multiple factors. The first can be the lower densities of the GNPs compared to the same fractional loading of CNTs in the Al6061 matrix. Lower density also means higher porosity and material lack compactness thus resulting in lower hardness in comparison with the same loading of CNTs. However, compared to the reference sample, the absence of a second phase (reinforcement) results in ductile and comparatively softer material.

The second reason can be associated with agglomeration/lumps of GNPs compared to the CNT clusters. CNTs tend also to cluster in absence of applied dispersion energy [43]. Based on these facts, a model can be perceived regarding absorption of energy level to deform or ability to resist deformation (Fig. 6).

The morphological effect of linear CNTs and 2D GNPs is the main reason for strain fields in the Al6061 matrix. Dispersion of the same weight fraction of CNTs and GNPs results in a high number density of CNTs as compared to the GNPs as later has sheet-type morphology. Thus, higher energy is absorbed by the CNT composites compared to GNP reinforced and the reference sample. This results in a decrease in ductility of the matrix and higher hardness and this is shown schematically in Fig. 6.

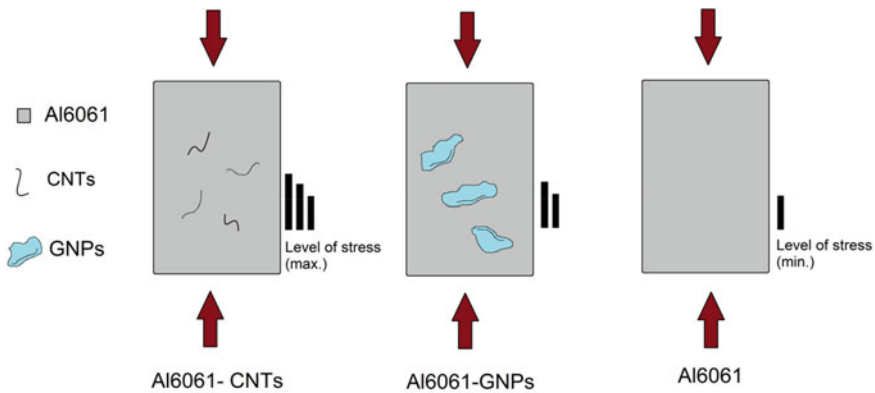


Fig. 6 Model depicting stress levels of energy required to resist deformation for CNT and GNP reinforced composites compared with the reference sample

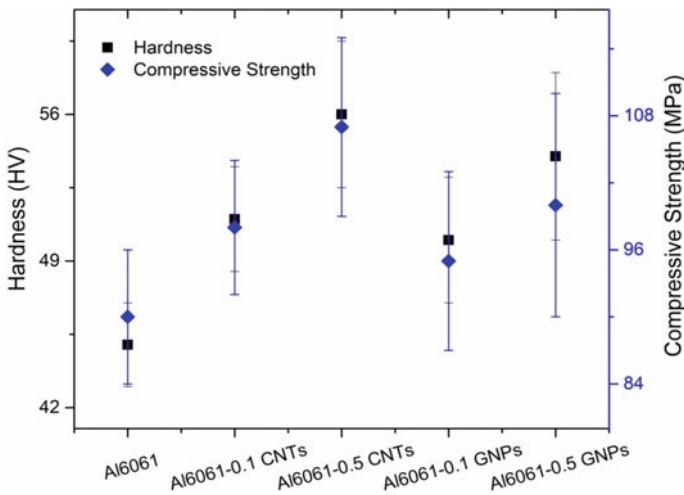


Fig. 7 Vickers hardness plotted with variation in CNT and GNP content

Compression Test

Figure 8 shows the compressive tests stress-strain curves of the reference samples, CNT and GNP composites. Four samples of each composition were tested to compare the compression test data. Table 2 shows compressive yield strength (CYS) values of reference samples and all the composites. As the compression strain was measured by the crosshead movement, the stress-strain data is plotted from the requisite behaviour of plasticity and failure. The initial elasticity has been cropped to focus the readers on the deformation behaviour in Fig. 8. The reference samples exhibited a CYS of 90 MPa in as-fabricated conditions. Addition of 0.1 wt.% CNTs increased the compressive strength of the composite to 98 MPa, which is a ~9% increase. Further addition up to 0.5 wt.% further increased the CYS to 18.9%, owing to the uniform dispersion of CNTs in the Al6061 matrix. The incremental increase in CYS was also observed for 0.1 and 0.5 wt.% addition of GNPs up to ~6% and 11%, respectively. The results are in accordance with Yang et al. [44] in Al-20Si alloy-matrix composites.

Common incremental behaviour in CYS was observed, however the failure strain remains morphological dependent. The reference samples exhibited excellent ductility by non-failure to the safe plunger limit threshold (i.e., >50%). The CNT composites were second to exhibit sufficiently high deformation without fracturing up to 35 and 24% with 0.1 and 0.5 wt.% addition, respectively. Contrary to CNTs, GNPs exhibited comparatively lower failure strain values. The equivalent content of GNPs as CNTs (0.1 wt.%) failed 25%, whereas the highest 0.5 wt.% of GNPs failed

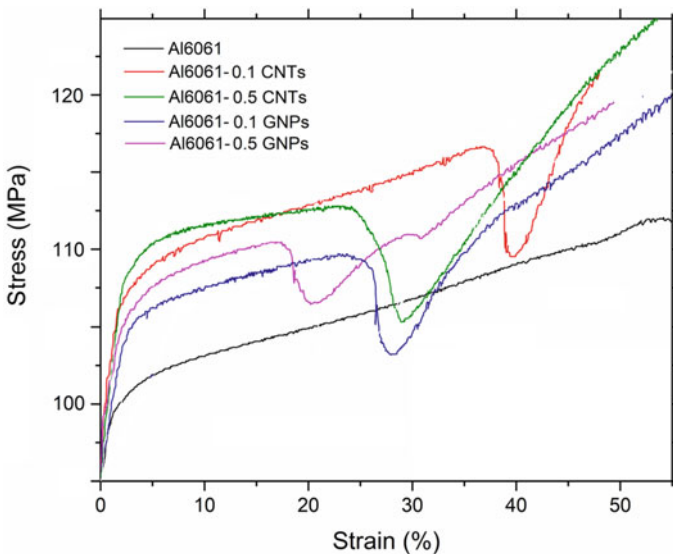


Fig. 8 Compression tests stress-strain curves of the reference, Al6061-CNT and Al6061-GNP composites

at 18% lowest ductility value. The contributing factor in this reduction of plasticity in GNP reinforced composites is lack of metallic density as can be seen from Fig. 3.

Increasing strain hardening balanced by the reduced plasticity is an energy conservative approach which both the composites are exhibiting due to their load-bearing capacity and interaction of second phase reinforcements with the dislocations. Therefore, a general trend of incremental strength is linked with a certain limit of reinforcement addition. The porosity in the material allows the migration of reinforcement under stress during bulk deformation. In other words, the crack propagation in principle direction tends to move/drag the reinforcement hindering the parting surfaces. A model has been developed as shown in Fig. 9 to depict the situation which tends to lower the failure strain in comparison with the same content of reinforcement with different/linear morphology. The linear, one-dimensional morphology of CNTs allows the crack to pass through it while the locked edges of the CNTs create a bridging effect [45]. This results in additional resistance to the crack propagation as shown in Fig. 9, Stage 2. A prominent bridge effect can be observed in stage 3 of the same nanoreinforcement. Compared to GNPs the situation may change after stage 2, as can be perceived, the 2D sheets may lump together due to the drag force of the propagating crack and at Stage 3 of GNPs, an open pathway like crack opening may appear. This allows the lower strain to create surfaces. Thus, a comparatively lower CYS and lower failure strain are observed for the GNP reinforced composites.

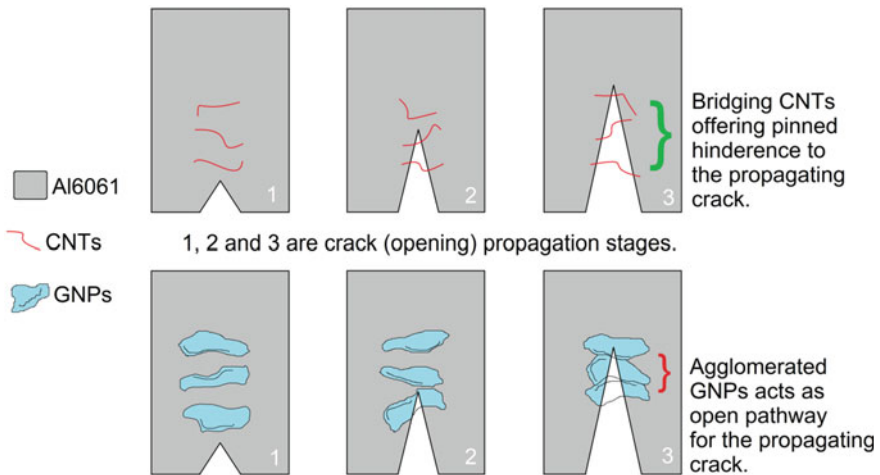


Fig. 9 Model illustration showing the restricted and pathway movement of the propagating crack through the Al6061 matrix in presence of CNTs and GNPs, respectively

Fractography

Figure 10 shows the fractured surfaces after the compression test, except for the reference samples, as they did not fail up to 60% plastic deformation. However, the pressed samples were shared with pliers to be compared with the other composite fractured surfaces. All the CNT and GNP composites also exhibited excellent ductility except for the square edges which sheared off and cracked at higher compressive stress. The fractography of these samples was conducted from fractured edges. Severely deformed grains with typical cup and cone morphology are evident of excellent ductility exhibited by the reference samples owning the near-theoretical density achieved by the SPS (Fig. 10a).

The addition of 0.1 and 0.5 wt.% CNTs did not change the morphology of the typical fracture pertaining to the reference samples. Tracing 0.1 wt.% CNTs in the fractures surfaces was extremely difficult, however in 0.5 wt.% some traces were identified and marked with red arrows in Fig. 10b. The model presented in Fig. 9 Stage 3 shows a typical condition as an actual witness in Fig. 10b. The bulged out CNTs (marked with red arrows) indicated the resistance to cracks deviating from the principal axis and causing a crack arrest situation of stage 2 in Fig. 10b.

Addition of 0.1 wt.% GNPs in the ductile aluminium matrix partially resulted in a decrease in plasticity. This reduction can be associated with the deviation from near-theoretical density and porosity between the GNP layers. Pulled out GNPs

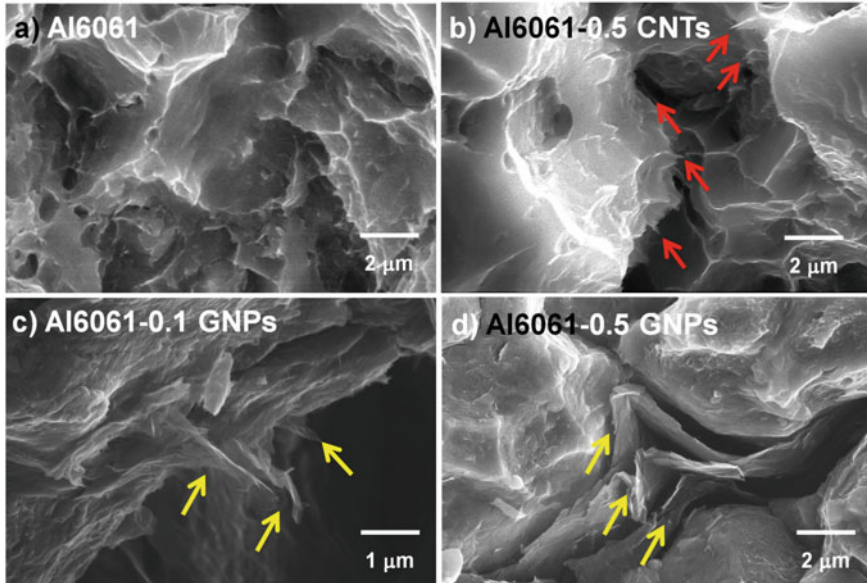


Fig. 10 SEM images of fractured surfaces of **a** Al6061 reference sample, **b** Al6061-0.5 CNTs, **c** Al6061-0.1 GNPs, and **d** Al6061-0.5 GNPs

encountered due to resisting a branching crack is shown in Fig. 11c. The GNPs are pointed by yellow arrows. In Fig. 10d, the fractured surface of Al6061-0.5 GNPs composite is shown with Stage 3 of Fig. 9, representing the GNPs lumping together to form a cavity type of pathway for the propagating crack. As the crack passes through the Al6061 matrix grains, under the incremental load, it encounters GNPs which hinder the forwarding crack until the applied force is superseding the GNPs trapped force between the Al6061 grains and hence meet the sliding. The number of uniformly distributed CNTs is higher than the GNPs in same wt.% in the matrix to offer higher pinning effect. Thus, overall higher load-bearing capacity is observed for the CNT composites compared with GNPC reinforced composites of the same composition. The increased CYS supports the assumption of nanoreinforcements movement and cracks resistance, as illustrated by the models presented in the present study. These models help to understand physical phenomena governing the strengthening mechanism of composites processed via SPS.

Conclusions

The CNT and GNP composites demonstrated improved mechanical properties in the aluminium alloy (Al6061) matrix. A comparative approach was adopted to evaluate their contribution in the strengthening of the bulk composite with a detailed investigation on the microstructural evolution and employment of SPS, as a processing method. The effects of SPS processing are correlated with the evolved microstructure and mechanical performance of the composites under compressive loading. The results are promising and would help researchers to assess the mechanism governing the potential use of CNT and GNP composites futuristic applications in the automobile and aerospace industries. The following conclusions can be drawn from the proceeding study:

1. SEM images of the ball-milled CNT- and GNP-powdered composites revealed the effectiveness of the dual dispersion technique.
2. The reference and composite samples possessed near-theoretical densities owing to the better compaction and sintering during SPS.
3. The evolved microstructure of the reference and composites samples revealed uniform distribution of the nanoreinforcements in the Al6061 matrix.
4. XRD did not reveal the presence of any interfacial phase or intermetallics.
5. The grain size reduction was apparent due to the uniform distribution of carbonaceous nanoreinforcements wrapped around the matrix grains.
6. The hardness of the Al6061 composites showed an increase with the addition of CNTs and GNPs.
7. The compression test results exhibited the same hardness test result's trend and revealed excellent plasticity of all the reference and composite samples. The interaction with dislocation at the nanolevel and grain refinement can be the responsible factor aided by bridging and anchoring the deformation.

8. The comparatively higher contribution of CNTs toward mechanical properties improvement with the same percentage weight fraction in the aluminium matrix is predominantly due to comparatively higher densities and lesser porosity associated with the linear, one-dimensional morphology.
9. The fractography revealed severely deformed grains of the reference and composite samples. Pulled out CNTs and GNPs were found evenly scattered in the micrographs.
10. A model is proposed to depict the deformation resistance elaborating the movement of crack and the response of carbonaceous nanoreinforcements.

Acknowledgements The authors acknowledge the financial support of the Higher Education Commission of Pakistan (grant no. 213-53249-2EG2-102) provided under the PhD indigenous fellowship; Phase-II Batch-II, as well as the Norwegian University of Science and Technology (NTNU), Norway, for the use of their laboratory facilities for processing and characterization.

Conflict of Interest All the authors declare hereby that they have no conflict of interest. The authors also declare that they have no known competing financial interests or personal relationships that could have appeared to influence the work reported in this paper.

References

1. Khan M, Amjad M, Khan A, Ud Din R, Ahmad I, Subhani T (2017) Microstructural evolution, mechanical profile, and fracture morphology of aluminum matrix composites containing graphene nanoplatelets. *J Mater Res* 32(11):2055–2066
2. Chen B, Kondoh K, Imai H, Umeda J, Takahashi M (2016) Simultaneously enhancing strength and ductility of carbon nanotube/aluminum composites by improving bonding conditions. *Scr Mater* 113:158–162
3. Chen L, Qi Y, Fei Y, Du Z (2020) Enhanced mechanical properties and thermal conductivity for GNPs/Al2024 composites with in situ SiC nanorods. *Met Mater Int* 27(10):4263–4270
4. Khan M, Rehman A, Aziz T, Shahzad M, Naveed K, Subhani T (2018) Effect of inter-cavity spacing in friction stir processed Al 5083 composites containing carbon nanotubes and boron carbide particles. *J Mater Proc Technol* 253:72–85
5. Khan M, Rehman A, Aziz T, Naveed K, Ahmad I, Subhani T (2017) Cold formability of friction stir processed aluminum composites containing carbon nanotubes and boron carbide particles. *Mater Sci Eng A* 696:552–557
6. Khan M, Ud Din R, Wadood A, Husain SW, Akhtar S, Aune RE (2020) Physical and mechanical properties of graphene nanoplatelet-reinforced Al6061-T6 composites processed by spark plasma sintering. *JOM* 72(6):2295–2304
7. Khan M, Ud Din R, Basit MA, Wadood A, Husain SW, Akhtar S, Aune RE (2021) Study of microstructure and mechanical behaviour of aluminium alloy hybrid composite with boron carbide and graphene nanoplatelets. *Mater Chem Phys* 271:124936
8. Khan M, Syed WH, Akhtar S, Aune RE. Friction stir processing (FSP) of multiwall carbon nanotubes and boron carbide reinforced aluminum alloy (Al 5083) composites. *Frict Stir Weld Process X*, pp 217–232
9. Khan M, Ud Din R, Abdul Basit M, Wadood A, Wilayat Husain S, Akhtar S, Aune R (2021) Effects of graphene nanoplatelets and boron carbide on microstructure and mechanical behaviour of aluminium alloy (Al6061) after friction stir welding. *Adv Mater Process Technol* 1–17

10. Khan M, Ud Din R, Wadood A, Syed WH, Akhtar S, Aune RE (2019) Effect of graphene nanoplatelets on the physical and mechanical properties of Al6061 in fabricated and T6 thermal conditions. *J Alloys Comp* 790:1076–1091
11. Zhou YT, Zan YN, Zheng SJ, Wang QZ, Xiao BL, Ma XL, Ma ZY (2017) Distribution of the microalloying element Cu in B4C-reinforced 6061Al composites. *J Alloys Comp* 728:112–117
12. Ravi B, Naik BB, Prakash JU (2015) Characterization of aluminium matrix composites (AA6061/B4C) fabricated by stir casting technique. *Mater Today Proc* 2(4–5):2984–2990
13. Ipekoglu M, Nekouyan A, Albayrak O, Altintas S (2017) Mechanical characterization of B4C reinforced aluminum matrix composites produced by squeeze casting. *J Mater Res* 32(3):599–605
14. Tan X-F, Zeng F-H, Wang S-Q, Zhou F, Xiong X (2014) Effects of heat treatment on phase contents and mechanical properties of infiltrated B4C/2024Al composites. *Trans Nonferrous Met Soc China* 24(7):2359–2365
15. Khan M, Ud Din R, Syed WH, Akhtar S, Aune RE (2019) Spark plasma sintering of boron carbide reinforced aluminum alloy (Al6061) matrix composites. In: *Proceedings of 2019 16th International Bhurban Conference on Applied Sciences & Technology (IBCAST)*, pp 35–41
16. Prashantha Kumar HG, Anthony Xavier M, Joel AP, Kaustav Chakraborty J (2018) Effect of flake reinforcement on mechanical properties of AA 6061 nano composite with secondary nano platelet-Graphene processed through powder metallurgy. *Mater Today Proc* 5(2), Part 2:6626–6634
17. Khan M, Zulfaqar M, Ali F, Subhani T (2017) Microstructural and mechanical characterization of hybrid aluminum matrix composite containing boron carbide and Al-Cu-Fe quasicrystals. *Met Mater Int* 23(4):813–822
18. Khan M, Zulfaqar M, Ali F, Subhani T (2017) Hybrid aluminium matrix composites containing boron carbide and quasicrystals: manufacturing and characterization. *Mater Sci Technol* 33(16):1955–1963
19. Ramesh CS, Keshavamurthy R, Madhusudhan J (2014) Fatigue behavior of Ni-P coated Si3N4 reinforced Al6061 composites. *Proc Mater Sci* 6:1444–1454
20. Chen HS, Wang WX, Li YL, Zhang P, Nie HH, Wu QC (2015) The design, microstructure and tensile properties of B4C particulate reinforced 6061Al neutron absorber composites. *J Alloys Comp* 632:23–29
21. Abdollahi A, Alizadeh A, Baharvandi HR (2014) Dry sliding tribological behavior and mechanical properties of Al2024–5 wt.%B4C nanocomposite produced by mechanical milling and hot extrusion. *Mater Des* 55:471–481
22. Zhang H, Ramesh KT, Chin ESC (2004) High strain rate response of aluminum 6092/B4C composites. *Mater Sci Eng A* 384(1–2):26–34
23. Khan M, Ahmad S, Zaidi S, Wadood A, Subhani T, Akhtar S, Husain SW, Aune RE (2020) Titanium carbide coating on graphene nanoplatelets. *J Mater Res Technol* 9(3):3075–3083
24. Abbas Shafqat Q, Rafi-Ud-Din U, Shahzad M, Khan M, Mehmood S, Syed WA, Basit A, Mehboob N, Ali T (2019) Mechanical, tribological, and electrochemical behavior of hybrid aluminum matrix composite containing boron carbide (B4C) and graphene nanoplatelets. *J Mater Res* 34(18):3116–3129
25. Khan M, Ud-Din R, Wadood A, Syed WH, Akhtar S, Aune RE. Spark plasma sintering of graphene nanoplatelets reinforced aluminium 6061 alloy composites, pp 301–311
26. Bisht A, Srivastava M, Kumar RM, Lahiri I, Lahiri D (2017) Strengthening mechanism in graphene nanoplatelets reinforced aluminum composite fabricated through spark plasma sintering. *Mater Sci Eng A* 695:20–28
27. Lian Y, Yang Z, Yang J, Mao C (2006) Processing and mechanical properties of 2024 aluminum matrix composites containing Tungsten and Tantalum prepared by PM. *Rare Met* 25(6), Supplement 2:136–140
28. Jiang Y, Song H, Xu R (2018) Research on the dispersion of carbon nanotubes by ultrasonic oscillation, surfactant and centrifugation respectively and fiscal policies for its industrial development. *Ultrason Sonochem* 48:30–38

29. Liu W-W, Xia B-Y, Wang X-X, Wang J-N (2012) Exfoliation and dispersion of graphene in ethanol-water mixtures. *Front Mater Sci* 6(2):176–182
30. Ju J-M, Wang G, Sim K-H (2017) Facile synthesis of graphene reinforced Al matrix composites with improved dispersion of graphene and enhanced mechanical properties. *J Alloys Comp* 704, Supplement C:585–592
31. Ud Din R, Shafqat QA, Asghar Z, Zahid GH, Basit A, Qureshi AH, Manzoor T, Nasir MA, Mehmood F, Hussain KI (2018) Microstructural evolution, powder characteristics, compaction behavior and sinterability of Al 6061–B4C composites as a function of reinforcement content and milling times. *Russ J Non-Ferr Met* 59(2):207–222
32. Chawla N, Chawla KK (2013) *Metal matrix composites*. Springer, New York
33. Liu J, Khan U, Coleman J, Fernandez B, Rodriguez P, Naher S, Brabazon D (2016) Graphene oxide and graphene nanosheet reinforced aluminium matrix composites: Powder synthesis and prepared composite characteristics. *Mater Des* 94:87–94
34. Khan M, Ud Din R, Wadood A, Husain SW, Akhtar S, Aune RE (2020) Physical and mechanical properties of graphene nanoplatelet-reinforced Al6061-T6 composites processed by spark plasma sintering. *JOM* 72(6):2295–2304
35. Zhang H, Xu C, Xiao W, Ameyama K, Ma C (2016) Enhanced mechanical properties of Al5083 alloy with graphene nanoplates prepared by ball milling and hot extrusion. *Mater Sci Eng A* 658:8–15
36. Liu G, Zhao N, Shi C, Liu E, He F, Ma L, Li Q, Li J, He C (2017) In-situ synthesis of graphene decorated with nickel nanoparticles for fabricating reinforced 6061Al matrix composites. *Mater Sci Eng A* 699, Supplement C:185–193
37. Tian W-M, Li S-M, Wang B, Chen X, Liu J-H, Yu M (2016) Graphene-reinforced aluminum matrix composites prepared by spark plasma sintering. *Int J Miner Metall Mater* 23(6):723–729
38. Bastwros M, Kim G-Y, Zhu C, Zhang K, Wang S, Tang X, Wang X (2014) Effect of ball milling on graphene reinforced Al6061 composite fabricated by semi-solid sintering. *Compos Part B: Eng* 60, Supplement C:111–118
39. Yolshina LA, Muradymov RV, Korsun IV, Yakovlev GA, Smirnov SV (2016) Novel aluminum-graphene and aluminum-graphite metallic composite materials: synthesis and properties. *J Alloys Comp* 663:449–459
40. Salama EI, Abbas A, Esawi AMK (2017) Preparation and properties of dual-matrix carbon nanotube-reinforced aluminum composites. *Compos Part A Appl Sci Manuf* 99:84–93
41. Latief FH, Sherif E-SM, Almajid AA, Junaedi H (2011) Fabrication of exfoliated graphite nanoplatelets-reinforced aluminum composites and evaluating their mechanical properties and corrosion behavior. *J Anal Appl Pyrol* 92(2):485–492
42. El-Rayes MM, El-Danaf EA (2012) The influence of multi-pass friction stir processing on the microstructural and mechanical properties of Aluminum Alloy 6082. *J Mater Process Technol* 212(5):1157–1168
43. Najimi AA, Shahverdi HR (2017) Microstructure and mechanical characterization of Al6061-CNT nanocomposites fabricated by spark plasma sintering. *Mater Charact* 133, Supplement C:44–53
44. Yang W, Chen G, Qiao J, Liu S, Xiao R, Dong R, Hussain M, Wu G (2017) Graphene nanoflakes reinforced Al-20Si matrix composites prepared by pressure infiltration method. *Mater Sci Eng A* 700, Supplement C:351–357
45. Shin SE, Bae DH (2018) Fatigue behavior of Al2024 alloy-matrix nanocomposites reinforced with multi-walled carbon nanotubes. *Compos Part B Eng* 134, Supplement C:61–68